Multifractality of correlated two-particle bound states in quasiperiodic chains

Diana Thongjaomayum,[1] Sergej Flach,[1,2] and Alexei Andreanov[1,2]
[1]*Center for Theoretical Physics of Complex Systems, Institute for Basic Science (IBS), Daejeon 34126, Korea*
[2]*Basic Science Program, Korea University of Science and Technology (UST), Daejeon 34113, Korea*

(Received 3 March 2020; accepted 13 April 2020; published 4 May 2020)

We consider the quasiperiodic Aubry-André chain in the insulating regime with localized single-particle states. Adding local interaction leads to the emergence of extended correlated two-particle bound states. We analyze the nature of these states, including their multifractality properties. We use a projected Green function method to compute numerically participation numbers of eigenstates and analyze their dependence on the energy and the system size. We then perform a scaling analysis. We observe multifractality of correlated extended two-particle bound states, which we confirm independently through exact diagonalization.

DOI: 10.1103/PhysRevB.101.174201

I. INTRODUCTION

Understanding the transport properties of quantum disordered or inhomogeneous systems has been an active topic of research since the discovery of Anderson localization (AL). AL describes the arrest of transport in a single-particle system due to disorder or inhomogeneous potential, which renders all the eigenstates in one and two space dimensions exponentially localized [1]. The original work of Anderson triggered a sequence of theoretical studies, and by now the single-particle case is well understood [2]. The important and much harder question involves the stability of modification of AL in the presence of many-body interactions. Decades of research attempts culminated in the opening of the field of many-body localization (MBL) [3–5]. Interestingly, one of the strongly debated issues is the possible existence of "bad" metallic states that are nonergodic or simply multifractal [3,5].

A notorious issue with MBL-related studies is the computational complexity due to the exponential proliferation of the Hilbert space dimension with increasing numbers of particles and system size. A legitimate and complementary approach is therefore to consider only a few interacting particles, which allows us to increase the system size beyond the limits set by typical MBL models. Three main directions with single-particle localization in one dimension have been explored: genuine AL due to uncorrelated disorder [2], Wannier-Stark localization (WSL) due to an external dc field [6], and Aubry-André localization (AAL) due to a quasiperiodic external potential [7]. Genuine AL yields a nontrivial increase of the localization length for two interacting particles with still unsettled scaling details [8–11]. Two interacting particles yield no localization change for WSL with interaction, only affecting the Bloch oscillation periods [12]. At variance, AAL with quasiperiodic potentials showed an unexpected transition from localization (zero interaction) to delocalization (nonzero interaction) [13]. These findings were later confirmed in Ref. [14], which provided additional indications for the fractal nature of the delocalized eigenstates.

Are these the seeds of a bad metal and the MBL transition from above? A hint might be obtained from the striking similarity of the phase diagram of correlated metallic two-particle bound states in Fig. 4 of Ref. [13] and the phase diagram of an MBL phase, which was experimentally assessed for interacting fermions in optical quasiperiodic potentials in Fig. 4 of Schreiber *et al.* in Ref. [15]. In the present study, we attempt to add more conclusive arguments that are aimed at a positive answer for the above question for quasiperiodic potentials. We confirm the fractal character of the two-particle spectrum and the fractality of some of the two-particle states. We rely on the projected Green function method [16], originally developed to analyze the localization length of two interacting particles in the AL case. The paper is organized as follows: We introduce the tools and other necessary means in Sec. II. Section III benchmarks these tools in the single-particle case against the exact results and exact diagonalization. In Sec. IV we analyze the case of two interacting particles. This is followed by conclusions.

II. SETTING THE STAGE

The starting point is a single particle placed in a quasiperiodic potential with the Aubry-André Hamiltonian [7]

$$\mathcal{H}_0 = \sum_n (|n\rangle\langle n+1| + \text{H.c.}) + \sum_m h_m |m\rangle\langle m|,$$
$$h_n = \lambda \cos(2\pi\alpha n + \beta), \tag{1}$$

where λ is the strength of the potential, and α is an irrational number ensuring quasiperiodicity of the potential. We choose $\alpha = (\sqrt{5}-1)/2$, the golden ratio, and we fix the hopping strength $t = 1$. Depending on the strength of the potential λ, the eigenstates are all delocalized ($\lambda < 2$) or localized ($\lambda > 2$) with localization length $\xi_1 = 1/\ln(\lambda/2)$, which is the same for all the eigenstates [7]. Finally, β is a phase that can be varied to generate different realizations of the quasiperiodic potential. In numerical studies with a finite system size, the choice of β will affect localized and sparse, fractal or multifractal extended states. In the present study involving critical states, we use averaging over different values of β, which we denote as $\overline{\cdots}$, to improve statistics.

We now add the interactions and consider two interacting bosons. We choose the on-site Hubbard interaction of strength u. The total Hamiltonian is given by

$$\begin{aligned}\mathcal{H} &= \mathcal{H}_0 \otimes \mathcal{H}_0 + uP \\ &= \sum_{n,m} (|n,m\rangle\langle n+1,m| + |n,m\rangle\langle n,m+1| + \text{H.c.}) \\ &\quad + \sum_{n,m} (h_n + h_m)\,|n,m\rangle\langle n,m| + uP, \end{aligned} \tag{2}$$

where $|n,m\rangle$ is a basis state with two particles at site n,m, and h_n is the on-site Aubry-André potential at site n given by Eq. (1). P is the projection operator defined as $P|n,m\rangle = \delta_{nm}|n,m\rangle$ that enforces the on-site Hubbard interaction.

The authors of the work Ref. [13] used exact diagonalization and unitary evolution of wave packets to study the two-particle properties of the model (2). The exact diagonalization limited the largest system sizes achievable to $N \approx 250$, imposed by the efficiency of full diagonalization of the Hamiltonian matrix (2). Later, Frahm in Ref. [14] implemented a dedicated sparse diagonalization algorithm based on Green functions [16,17] to handle large sizes, up to $N = 10\,946$, of the Hamiltonian (2). We follow the original approach of Ref. [16]. We extract the relevant two-particle properties from the projected two-particle Green function, which is obtained as a projection of the full Green function $G = (E - \mathcal{H})^{-1}$ onto doubly occupied states (relying crucially on the fact that the Hubbard interaction is proportional to the projector P):

$$\tilde{G} = \frac{\tilde{G}_0}{1 - u\tilde{G}_0}. \tag{3}$$

Here $\tilde{G} = PGP$ and $\tilde{G}_0 = PG_0P$; G_0 is the noninteracting two-particle GF, which can be obtained by straightforward diagonalization of the single-particle Hamiltonian (1). Knowing the single-particle eigenenergies $\{E_\mu\}$ and eigenfunctions $\{\phi_\mu(n)\}$, we compute G_0 as follows:

$$\begin{aligned}\langle n,n|G_0(E)|m,m\rangle &= \sum_{\mu,\nu} \frac{\phi_\mu(n)\phi_\nu(n)\phi^*_\mu(m)\phi^*_\nu(m)}{E - E_\mu - E_\nu} \\ &= \sum_\mu \phi_\mu(n) g_0(E - E_\mu)\phi_\mu(m), \\ g_0(E) &= \frac{1}{E - \mathcal{H}_0} = \sum_\nu \frac{\phi^*_\nu(n)\phi_\nu(m)}{E - E_\nu}. \end{aligned} \tag{4}$$

The reordering of the terms in the second line is done to reduce the complexity of the computation from the original $O(N^4)$ to $O(N^3)$ [9], since the single-particle Green function g_0 can be efficiently evaluated using tridiagonal matrix inversion of the single-particle Hamiltonian (1). This approach allows us achieve system sizes as large as $N = 7000$.

In the insulating regime, the exponential decay of the projected Green's function $\tilde{G}$ was used to extract the localization length of two interacting particles (TIPs) [11,16,18]. Here we are aiming to investigate TIP eigenstates that we expect to be extended in a predominantly insulating region [13], therefore $\tilde{G}$ might not decay or the decay might not be exponential. Consequently, we adopt a different measure [11]: Interpreting the projected Green function $\tilde{G}$ as a probability density function, we define the participation number $I_{q=2}$ and its higher moments $I_{q>2}$ as

$$I_q = \left(\sum_k |\tilde{g}(k)|\right)^q \Big/ \sum_k |\tilde{g}(k)|^q, \tag{5}$$

where $\tilde{g}(k) = \langle n,n|\tilde{G}|n+k,n+k\rangle$. We shall use I_2 and higher moments that are always well defined to analyze the TIP states. To distinguish I_q from the conventional participation number, we will refer to it as the Green function participation number (GPN). However, before we can proceed to the two-particle case, we need to confirm that I_2 is a valid measure of localization of an eigenstate Ψ, similar to the conventional participation number:

$$\text{PN}_q = \sum_{nm} |\Psi_{nm}|^{2q}, \tag{6}$$

e.g., that I_2 can distinguish between extended, (multi)fractal, and localized states.

III. SINGLE-PARTICLE: BENCHMARKING

To confirm that the above-defined participation number I_q is a valid probe of localization properties of eigenstates, we first consider the single-particle case. To achieve this, we benchmark two single-particle quantities: localization length—analytical and numerical,

$$\xi_1 = \frac{1}{\ln\left(\frac{\lambda}{2}\right)}, \tag{7}$$

$$\frac{1}{\xi_1} = -\lim_{|n-m|\to\infty} \frac{\overline{\ln|\langle n|g_0|m\rangle|}}{|n-m|}, \tag{8}$$

and participation number I_2, which is defined similarly to its two-particle version Eq. (5):

$$I_q = \left(\sum_k |g(k)|\right)^q \Big/ \sum_k |g(k)|^q, \tag{9}$$

where $g(k) = \langle n|g_0|n+k\rangle$. Our aim is to confirm that I_2 is a valid substitute for ξ_1 for localized states, and it behaves like the conventional participation number for localized and extended states.

To prove that, we consider three different values of the potential strength $\lambda = 1$, 2, and 2.5, which correspond to the delocalized, critical, and localized regimes, respectively. For each λ, we compute single-particle eigenstates ψ and the Green function g_0 for energies $E \in [-3,3]$ in steps of $\Delta E = 0.05$, scanning the entire single-particle spectrum. This step size of 0.05 is chosen to be slightly bigger than the level spacing $\delta(N = 250) = 0.004$ and $\delta(N = 500) = 0.002$ for the data presented in Fig. 1. From the Green function g_0 we evaluate ξ_1 and I_2, and from the eigenstates ψ we compute PN_2. Figure 1(a) shows the results for $\lambda = 1$ for which all the single-particle eigenstates are extended. The plot of Fig. 1(a) shows I_2 and PN_2 versus E for system sizes $N = 250, 500$. The bottom circular/blue points of Fig. 1(a) show the single-particle spectrum obtained from the full diagonalization of $\mathcal{H}_0$ for $N = 500$. We see that both participation numbers PN_2 and I_2 drop to zero in the gaps of the spectrum of $\mathcal{H}_0$, and they increase with the system size for energies where eigenstates

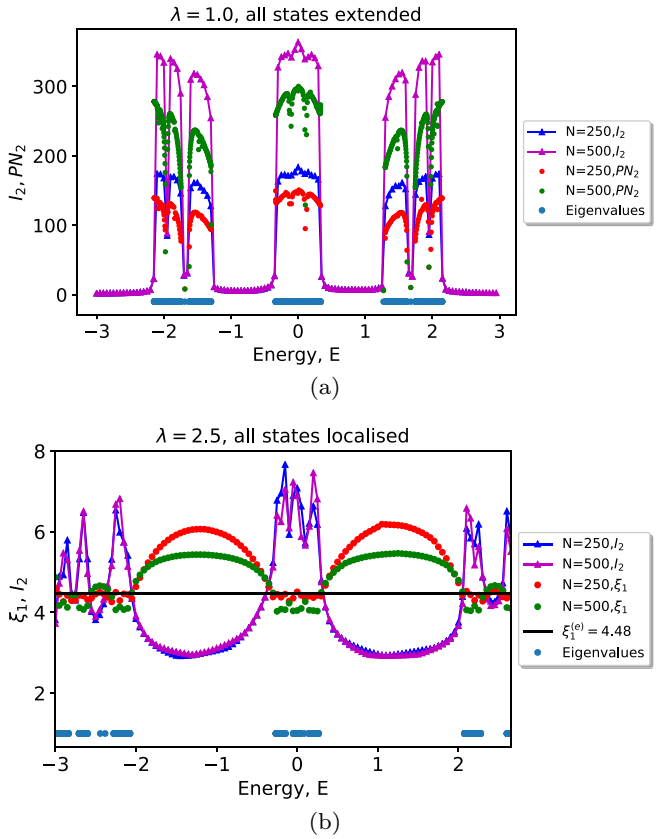

FIG. 1. Benchmarking of a single particle in the AA model: (a) $\lambda = 1$: I_2 and PN_2 for $N = 250, 500$. (b) $\lambda = 2.5$: Localization length ξ_1 and I_2 for $N = 250, 500$. The black line represents the analytical value $\xi_1 = 4.48$. The participation number PN_2 behaves similarly to I_2 (not shown). The bottom blue/circular points in both (a) and (b) represent the spectrum of $\mathcal{H}_0$ for $N = 500$ and show the locations of the eigenstates.

are present. We observe $I_2 > \mathrm{PN}_2$ in general [11]. Figure 1(b) compares the same quantities for $\lambda = 2.5$, where the entire spectrum is localized. Figure 1(b) shows I_2 and ξ_1 against E for $N = 250, 500$. The eigenenergies are plotted at the bottom of Fig. 1(b) (light blue points). The black line is the exact localization length $\xi_1^{(e)} = 1/\ln(1.25) \approx 4.48$. The localization length ξ_1 evaluated from the Green function (8) is close to the exact value $\xi_1^{(e)}$ for energies close to the eigenenergies of the system, while I_2 is systematically larger than ξ_1, but is roughly of the same order, and does not scale with the system size N. In the gaps of the exact spectrum, I_2 drops to zero, which is expected since there are no eigenstates corresponding to these energies, and contributions from the eigenstates are negligible. However ξ_1, defined by Eq. (8), gives a completely wrong value in the gaps of the single-particle spectrum as seen in Fig. 1(b). This is clearly an artefact of the exponential fitting of g_0 that does not decay exponentially inside the gaps of the spectrum of $\mathcal{H}_0$. The behavior of the participation number PN_2 is very similar to I_2 (not shown). For the critical case $\lambda = 2$, the behavior of ξ_1 and I_2 is similar to that of the delocalized $\lambda = 1$ case.

This rough comparison lends support to the validity of I_2 as a substitute for the participation number PN_2. To strengthen this support, we look into the scaling of the participation

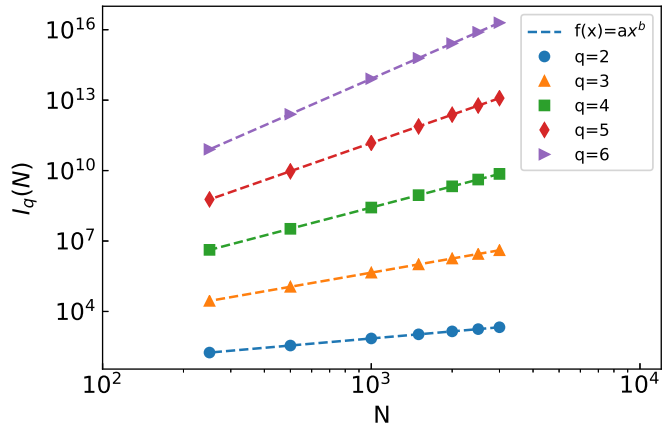

FIG. 2. Participation number $I_q(N)$ (symbols) vs system size $N = 250$–3000 for $q = 2, 3, 4, 5, 6$ and the power-law fits $I_q(N) = aN^b$ (dashed lines) for $\lambda = 1$. The power-law fit works well also for $\lambda = 2, 2.5$ (not shown).

numbers PN_q with the power q, which also distinguishes extended, localized, and (multi)fractal states: $\mathrm{PN}_q = aN^{\mathcal{D}_q(q-1)}$, where $\mathcal{D}_q$ is the fractal dimension of the state, and $\mathcal{D}_q = 0$ corresponds to localized states, $\mathcal{D}_q = 1$ corresponds to delocalized states, and $0 < \mathcal{D}_q < 1$ corresponds to (multi)fractal states. We verify whether a similar scaling holds for I_q, and we try the fit $I_q = aN^{D_q(q-1)}$ for all three regimes: $\lambda = 1, 2, 2.5$. We pick the energy $E_{\max}$ corresponding to the maximum of I_2 for the largest system size considered, $N = 3000$, since we want to probe the most delocalized states in an otherwise localized regime (this choice is only relevant for $\lambda = 2.5$, where all eigenstates are localized), and we use this value $E_{\max}$ to evaluate D_q for smaller system sizes. For every λ we compute I_q for $q = 2, 3, 4, 5, 6$ and for a range of system sizes

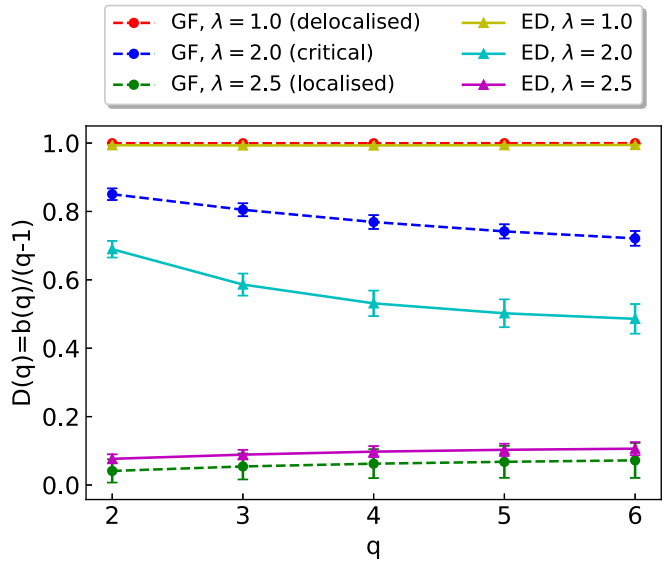

FIG. 3. Fractal dimension D_q vs q obtained from the Green's function (GF) and exact diagonalization (ED) in extended (red/yellow), critical (blue/cyan), and localized (green/magenta) regimes for the single-particle case. The dimension D_q is q-independent and equal to 0 (1) in the extended (localized) regime and has a nontrivial dependence on q at the criticality, $\lambda = 2$. This a similar behavior to the dimension $\mathcal{D}_q$ computed from the PN_q.

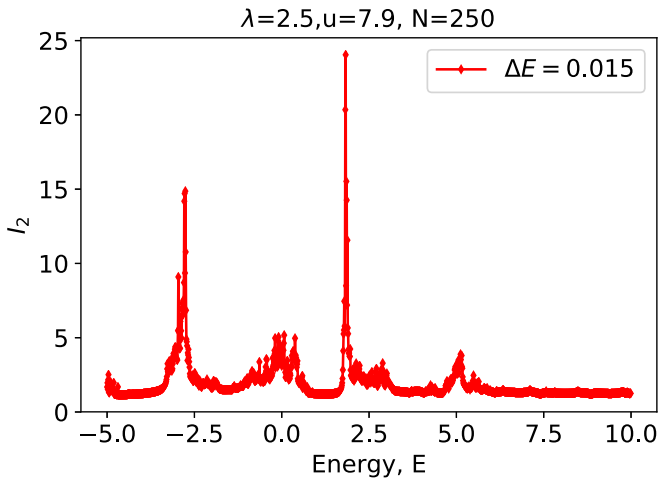

FIG. 4. Participation number I_2 vs energy E for two interacting particles. The peaks signal the emergence of delocalized states in the otherwise localized spectrum.

$N = 250$–3000. The results are shown in Fig. 2: we see a clear power-law scaling of I_q with N for every individual value of q. Next we fit these data for several system sizes to extract D_q for the values of $\lambda = 1, 2, 2.5$. Similarly we evaluate the $\mathcal{D}_q$ from the scaling of PN_q with system size. The PN_q are computed from exact diagonalization of a single-particle Hamiltonian (1). The results are summarized in Fig. 3: both methods agree—$\mathcal{D}_q \approx D_q \approx 1$ for $\lambda = 1.0$, as it should be for extended states; $\mathcal{D}_q \approx D_q \approx 0.0$ for the localized case $\lambda = 2.5$; and q-dependent $\mathcal{D}_q, D_q$ for the critical value $\lambda = 2.0$, where multifractality is expected.

These results indicate that I_2 can be used as a substitute for the localization length ξ_1 and the participation number PN_q in the single-particle case. We assume that this is also the case for two interacting particles, and we verify this assumption self-consistently. Therefore, in what follows we will study the behavior of I_2 and higher moments $I_{q>2}$.

IV. TWO INTERACTING PARTICLES: SELF-SIMILARITY OF THE SPECTRUM AND FRACTALITY OF THE EIGENSTATES

We now turn to the case of two particles with the on-site Hubbard interaction. Earlier work [13] has reported the emergence of metallic states in the single-particle insulating regime ($\lambda > 2$). This conclusion was based on exact diagonalization of systems up to $N = 250$ (up to $N = 1000$ with sparse diagonalization) sites and analysis of the spreading of time-evolved wave packets scanned in the entire range of interactions $0 < u < 12$ for several values of potential strength $\lambda \in [1.8, 3]$. These results were enhanced by Frahm [14], who performed diagonalization of systems up to $N = 10\,946$ sites and confirmed the presence of delocalized states.

We start our analysis with a cross-check of Ref. [13] and evaluate the participation number I_2 from $\tilde{G}_{nm}$ (5) for $\lambda = 2.5$, $u = 7.9$, and 1000 values of energy $E \in [-5, 10]$. The results are averaged over 10 disorder realizations, e.g., values of β; see Eq. (1). In Fig. 4 we see a miniband structure with the few energies where the value of I_2 is relatively large, similarly to the findings of Ref. [13], thereby lending further support to the use of I_2 as a probe of the extent of the eigenstates. We identified two values of energy, $E_1 \approx 1.8, E_2 \approx -2.8$, where I_2 achieves its local maximum (Fig. 4), suggesting the emergence of delocalized states at these energies.

To get a better insight into the nature of these emerging states, we study the fine structure in the vicinity of the I_2 peaks. To extract this fine structure, we start with a small system size and identify the peaks of I_2 by discretizing the energy range. Next we zoom into the energy range around one of the peaks by using a finer energy discretization. This procedure is repeated several times for increasing system sizes N. Such analysis of fine details of the structure of I_2 is possible thanks to the usage of the projected Green functions. To be specific for the peak of I_2 at $E_1 \approx 1.8$, we started with a range or energies [1.821 : 1.8225] for the smallest system size $N = 250$. We observe the emergence of new peaks, which become prominent as the size is increased to $N = 500$ and 1000 [Fig. 5(a)]. Zooming in the energy range around one peak ($E \in [1.8212, 1.8215]$, marked by black rectangular boxes in Fig. 5), the original peak resolves into several peaks for larger system size $N = 3000$, Fig. 5(b). Repeating this procedure two more times for the peaks marked by the black boxes, we obtain Figs. 5(c) and 5(d) for $N_{\max} = 7000$. The largest I_2 is observed at $E_1 = 1.821\,406\,3$ for $N = 7000$. Upon every iteration, we observe the emergence of finer structure in I_2 as we are zooming in energy. This strongly suggests the fractal nature of participation number I_2 as a function of energy E and consequently the spectrum of the delocalized states at these energies.

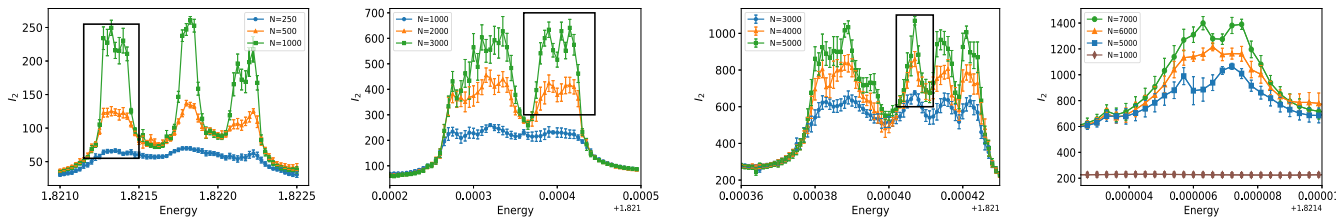

(a) (b) (c) (d)

FIG. 5. Average Green's function participation number I_2 around energy $E_1 \approx 1.8$ at $u = 7.9$. The energy range is zoomed in from left to right, with the maximum system size increasing from $N = 1000$ (left) to $N = 7000$ (right) and the resolution in energy reaching $\Delta E = 3 \times 10^{-7}$ for the rightmost plot. The errorbars correspond to the disorder average. The peaks of I_2 resolve into fine structure with subpeaks upon every iteration of zooming in.

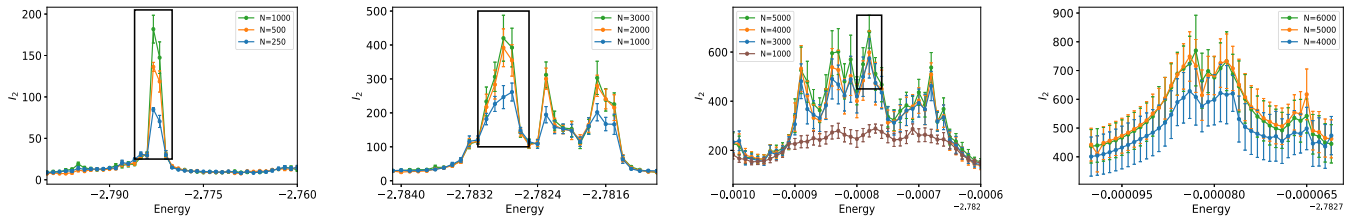

FIG. 6. Average Green's function participation number I_2 around energy $E_2 \approx -2.8$ at $u = 7.9$. The energy range is zoomed in from left to right, with the maximum system size increasing from $N = 1000$ (left) to $N = 6000$ (right) and the resolution in energy reaching $\Delta E = 10^{-6}$ for the rightmost plot. The errorbars correspond to the disorder average. The peaks of I_2 resolve into fine structure with subpeaks upon every iteration of zooming in.

In the original work, Ref. [13], these states were assumed delocalized based on the analysis of wave-packet spreading. Subsequent work in Ref. [14] performed a more detailed analysis and confirmed this conclusion and also provided some indications of fractality of these states based on the fitting (i) inverse participation ratio in position representation denoted as ξ_x, (ii) inverse participation ratio in energy representations, ξ_E (for details, see Ref. [14]). To clarify the fractal nature of these states, we consider the largest I_2 at energy $E = E_1$ and compute $I_q(N)$ for $q = 2, 3, 4, 5, 6$ and several system sizes N at this energy. Assuming the multifractal ansatz for the participation number $I_q(N) \sim aN^{D_q(q-1)}$, we extract the fractal dimension D_q from numerical values $I_q(N)$, similarly to how it was done in the single-particle case; see Fig. 2. The extracted values of D_q are shown as red points (circles) in Fig. 7 with the error bars of the fit. We observe that $D_q < 1$ and is q-dependent, suggesting that the corresponding eigenstates at this energy are multifractal. In Ref. [14], a power-law fit of ξ_x and ξ_E with system size N with $N_{\max} \approx 10\,000$ was computed. The extracted values of the power-law exponents $a_{x,E} < 1$ for energies $E = -2.787, 1.817$ and interaction $u = 7.9$ suggested that these states were fractal.

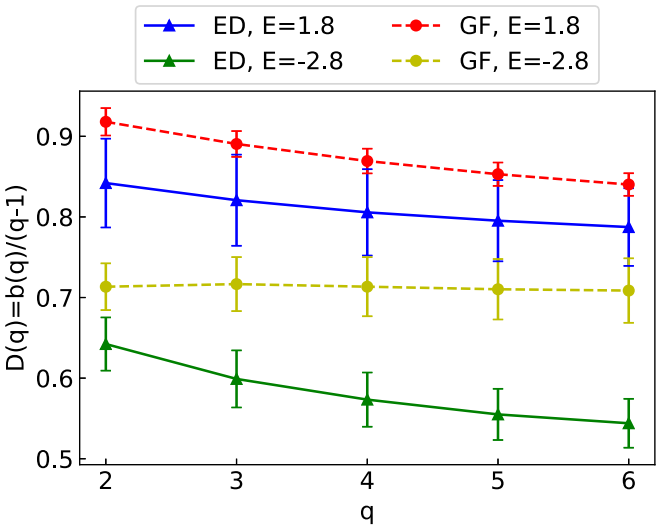

FIG. 7. Fractal dimensions D_q (extracted from the Green function participation number I_q) and $\mathcal{D}_q$ (extracted from the participation number PN_q) vs q at energies $E_1 \approx 1.8$ and $E_2 \approx -2.8$. For E_1 both methods predict multifractality, while for E_2 the projected Green function method underestimates the fractality of the eigenstate.

In the same way, energies around $E_2 \approx -2.8$ were analyzed, up to system size $N_{\max} = 6000$. The results were averaged over 10 disorder samples, e.g., values of β [see Eq. (1)]. The results are shown in Fig. 6. We observe larger fluctuations in participation number I_2 as compared to $E_1 \approx 1.8$, which are shown with the error bars. Also the dependence of I_2 on system size N is less prominent as compared to the global maximum of I_2 located at $E_1 \approx 1.8$ when the energy is zoomed in, even for the largest system size considered [Figs. 6(c) and 6(d)]. The fractal dimension D_q extracted from I_q shows an almost flat dependence on q (green circles in Fig. 7), suggesting only fractal but not multifractal character of the state at this energy.

The Green function participation number results are indirect, since they do not probe the eigenstates directly. Their advantage is the much lower computational cost for larger system sizes as compared to the exact diagonalization. Therefore, to check our predictions on the fractality of the eigenstates independently, we performed sparse diagonalization around energies $E_1 = 1.821\,406\,3$ and $E_2 = -2.782\,783$, corresponding to the local maxima of I_2 for $N_{\max} = 7000$ and 6000, respectively. Among the eigenstates extracted around these two energies, we systematically picked the ones with the largest PN_2 for all system sizes N since we aimed at the most delocalized eigenstates embedded in the predominantly localized ones. The power-law fits of the participation number moments, $\mathrm{PN}_q(N) \propto N^{\mathcal{D}_q(q-1)}$, were calculated. The resulting values of $\mathcal{D}_q$ are shown in Fig. 7 as blue ($E = 1.8$) and green ($E = -2.8$) solid lines with triangular points. The dashed lines with points show D_q evaluated from the Green function participation numbers, red for $E_1 = 1.8$ and yellow for $E_2 = -2.8$. We see that although the values of D_q and $\mathcal{D}_q$ do not always agree perfectly, nevertheless D_q and $\mathcal{D}_q$ imply at least fractality of the eigenstates that were previously considered delocalized [13]. This also provides still more evidence for the validity of I_q as a measure of localization of eigenstates.

We elaborate further on the character of these fractal states appearing around $E_{1,2}$. Since the appearance of these states relies crucially on the interaction, we expect them to have a peculiar spatial pattern of the wave-function amplitudes. Indeed we can construct many approximate localized eigenstates with two particles separated by one or more localization lengths ξ_1. Therefore, the fractal states should have the two particles separated by at most the single-particles localization length ξ_1. If we visualize the amplitudes of the two-particle eigenfunction $|\Psi(x_1, x_2)|$ on a square lattice with coordinates

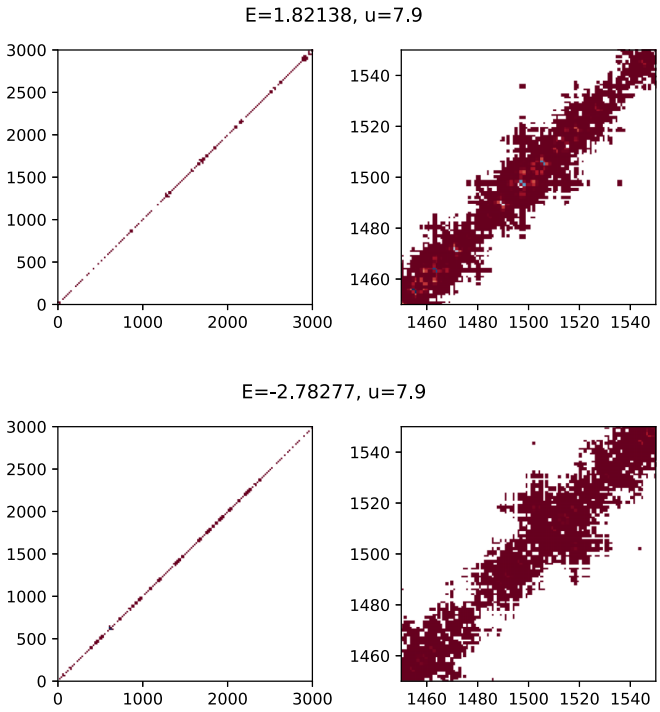

FIG. 8. The amplitudes $|\Psi(x_1, x_2)|$ of eigenstates computed for $N = 3000$ at $u = 7.9$ and corresponding to the local maxima of PN_2. The X-axis and Y-axis denote the positions of the two particles: x_1 and x_2, respectively. The larger amplitudes correspond to brighter color. Values smaller than 10^{-8} were discarded. The energies are $E_1 \approx 1.8$ (top) and $E_2 = -2.782\,77$ (bottom). Left column: The eigenstate is localized along the main diagonal, e.g., the two particles stick together, but the pattern of the amplitudes along the diagonal is multifractal. Right column: the zoom into the left figure, highlighting the complex, multifractal pattern of the eigenfunction along the diagonal.

x_1, x_2, which correspond to the positions of the two particles, we expect the fractal states to be localized along the main diagonal $x_1 = x_2$, the fractal structure translating into some complicated pattern along the main diagonal. To verify this hypothesis, we plotted two exact eigenstates with the largest PN_2 for $N = 3000$ in Fig. 8 [$u = 7.9$ and $E_1 \approx 1.8$ (top) and $E_2 \approx -2.78$]. The axes denote the position of each of the two particles. We truncated amplitudes $|\Psi(x_1, x_2)| < 10^{-8}$ on the plots. These plots fully confirm our hypothesis outlined above, with most weight concentrated along the main diagonal, i.e., both particles being close to each other.

V. CONCLUSIONS

To conclude, we have shown that previously discovered metallic states of two interacting particles in an AA chain in the insulating single-particle region have a fractal structure. Furthermore, unlike previous claims, we find that these states are multifractal. This is verified by computing participation numbers from the projected GF as well as from exact diagonalization. An interesting open problem is the fate of these multifractal states at finite density where many-body localization was reported at half-filling [19].

As a side effect, we demonstrated that the projected Green functions can be used as a first probe to check the nature of eigenstates in an interacting Hamiltonian system having the advantage that larger system sizes can be targeted as compared to the computationally challenging exact diagonalization.

ACKNOWLEDGMENT

This work was supported by the Institute for Basic Science in Korea (IBS-R024-D1).

[1] P. W. Anderson, Absence of diffusion in certain random lattices, Phys. Rev. **109**, 1492 (1958).
[2] B. Kramer and A. MacKinnon, Localization: theory and experiment, Rep. Prog. Phys. **56**, 1469 (1993).
[3] D.M. Basko, I.L. Aleiner, and B.L. Altshuler, Metal-insulator transition in a weakly interacting many-electron system with localized single-particle states, Ann. Phys. **321**, 1126 (2006).
[4] D. A. Abanin, E. Altman, I. Bloch, and M. Serbyn, Colloquium: Many-body localization, thermalization, and entanglement, Rev. Mod. Phys. **91**, 021001 (2019).
[5] F. Alet and N. Laflorencie, Many-body localization: An introduction and selected topics, C. R. Phys. **19**, 498 (2018).
[6] H. Fukuyama, R. A. Bari, and H. C. Fogedby, Tightly bound electrons in a uniform electric field, Phys. Rev. B **8**, 5579 (1973).
[7] S. Aubry and G. André, Analyticity breaking and Anderson localization in incommensurate lattices, Ann. Israel Phys. Soc. **3**, 133 (1980).
[8] D. L. Shepelyansky, Coherent Propagation of Two Interacting Particles in a Random Potential, Phys. Rev. Lett. **73**, 2607 (1994).
[9] K. M. Frahm, Interaction induced delocalization of two particles: large system size calculations and dependence on interaction strength, Eur. Phys. J. B **10**, 371 (1999).
[10] D. O. Krimer, R. Khomeriki, and S. Flach, Two interacting particles in a random potential, JETP Lett. **94**, 406 (2011).
[11] D. Thongjaomayum, A. Andreanov, T. Engl, and S. Flach, Taming two interacting particles with disorder, Phys. Rev. B **100**, 224203 (2019).
[12] R. Khomeriki, D. O. Krimer, M. Haque, and S. Flach, Interaction-induced fractional Bloch and tunneling oscillations, Phys. Rev. A **81**, 065601 (2010).
[13] S. Flach, M. Ivanchenko, and R. Khomeriki, Correlated metallic two-particle bound states in quasiperiodic chains, Europhys. Lett. **98**, 66002 (2012).
[14] K. M. Frahm and D. L. Shepelyansky, Freed by interaction kinetic states in the Harper model, Eur. Phys. J. B **88**, 337 (2015).
[15] M. Schreiber, S. S. Hodgman, P. Bordia, H. P. Lüschen, M. H. Fischer, R. Vosk, E. Altman, U. Schneider, and I. Bloch, Observation of many-body localization of interacting fermions in a quasirandom optical lattice, Science **349**, 842 (2015).

[16] F. von Oppen, T. Wettig, and J. Müller, Interaction-Induced Delocalization of Two Particles in a Random Potential: Scaling Properties, Phys. Rev. Lett. **76**, 491 (1996).

[17] W. E. Arnoldi, The principle of minimized iteration in the solution of the matrix eigenvalue problem, Quart. Appl. Math. **9**, 17 (1951).

[18] K. M. Frahm, Eigenfunction structure and scaling of two interacting particles in the one-dimensional Anderson model, Eur. Phys. J. B **89**, 115 (2016).

[19] S. Iyer, V. Oganesyan, G. Refael, and D. A. Huse, Many-body localization in a quasiperiodic system, Phys. Rev. B **87**, 134202 (2013).